



Structural basis for the sequestration of the anti- σ^{70} factor Rsd from σ^{70} by the histidine-containing phosphocarrier protein HPr

Young-Ha Park,^{a,‡} Si-Hyeon Um,^{b,‡} Saemeo Song,^b Yeong-Jae Seok^{a,c,*} and Nam-Chul Ha^{b,*}

Received 22 May 2015

Accepted 20 July 2015

Edited by C. S. Bond, University of Western Australia, Crawley, Australia

‡ These authors contributed equally to this work.

Keywords: HPr; Rsd; σ^{70} ; PTS; stationary phase.

PDB reference: HPr–Rsd complex structure, 4xwj

Supporting information: this article has supporting information at journals.iucr.org/d

^aDepartment of Biological Sciences and Institute of Microbiology, Seoul National University, Seoul 151-742, Republic of Korea, ^bDepartment of Agricultural Biotechnology, Center for Food Safety and Toxicology, Research Institute for Agricultural and Life Sciences, Seoul National University, Seoul 151-921, Republic of Korea, and ^cDepartment of Biophysics and Chemical Biology, Seoul National University, Seoul 151-742, Republic of Korea. *Correspondence e-mail: yjseok@snu.ac.kr, hanc210@snu.ac.kr

Histidine-containing phosphocarrier protein (HPr) is a general component of the bacterial phosphoenolpyruvate:sugar phosphotransferase system (PTS) involved in the phosphorylation-coupled transport of numerous sugars called PTS sugars. HPr mainly exists in a dephosphorylated form in the presence of PTS sugars in the medium, while its phosphorylation increases in the absence of PTS sugars. A recent study revealed that the dephosphorylated form of HPr binds and antagonizes the function of the antisigma factor Rsd. This anti-sigma factor sequesters the housekeeping sigma factor σ^{70} to facilitate switching of the sigma subunit on RNA polymerase from σ^{70} to the stress-responsive sigma factor σ^S in stationary-phase cells. In this study, the structure of the complex of Rsd and HPr was determined at 2.1 Å resolution and revealed that the binding site for HPr on the surface of Rsd partly overlaps with that for σ^{70} . The localization of the phosphorylation site on HPr at the binding interface for Rsd explains why phosphorylation of HPr abolishes its binding to Rsd. The mutation of crucial residues involved in the HPr–Rsd interaction significantly influenced the competition between HPr and σ^{70} for binding to Rsd both *in vitro* and *in vivo*. The results provide a structural basis for the linkage of global gene regulation to nutrient availability in the external environment.

1. Introduction

The phosphoenolpyruvate (PEP):sugar phosphotransferase system (PTS) plays a primary role in the uptake and phosphorylation of sugars in many bacteria (Postma *et al.*, 1993). The phosphoryl group of PEP is transferred to a sugar molecule as the sugar enters a cell *via* two general cytoplasmic components and one sugar-specific membrane-bound transporter (Postma *et al.*, 1993; Barabote & Saier, 2005). The first general component, enzyme I (EI), accepts the phosphoryl group from PEP and transfers it to the histidine-containing phosphocarrier protein HPr, which is the second general component. The phosphoryl group is then transferred from HPr to the sugar-specific transport complex enzyme II^{sugar} (EII^{sugar}). Within the EII complex, the phosphoryl group is sequentially transferred from the sugar-specific soluble subunit EIIA to the juxtamembrane subunit EIIB, which phosphorylates incoming sugar molecules through the transmembrane subunit EIIC.

Components of the PTS are also involved in signal transduction to couple sugar transport to the regulation of many cellular processes (Deutscher *et al.*, 2014). In the presence of glucose or other PTS sugars, the ratio of dephosphorylated

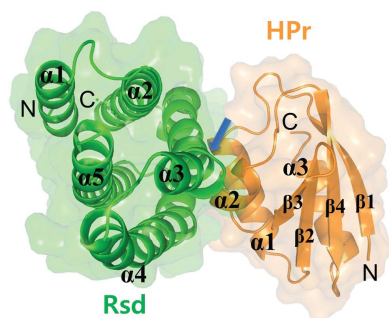


Table 1

E. coli strains and plasmids used in this study.

Strain or plasmid	Genotype or phenotype	Source or reference
Strains		
G1698	F ⁻ λ ⁻ <i>lacI^d lacPL8 ampC::P_{trp} cI</i>	LaVallie <i>et al.</i> (1993)
MG1655	Wild-type <i>E. coli</i> K-12	Blattner <i>et al.</i> (1997)
MG1655 Δ <i>rsd</i>	MG1655 <i>rsd::Tet^r</i>	Park <i>et al.</i> (2013)
ER2566	F ⁻ λ ⁻ <i>thua2 [lon] ompT lacZ::T7 gene 1 gal sulA11 Δ(mcrC-mrr)114::IS10 R(mcr-73::miniTn10-TetS)2 R(zgb-210::Tn10)(TetS) endA1 [dcm]</i>	NEB
ER2566 Δ <i>pts</i>	ER2566 <i>pts::Km^r</i>	Laboratory stock
Plasmids		
pRE1	Expression vector under control of λP _L promoter, Amp ^r	Reddy <i>et al.</i> (1989)
pSP100	pRE1-based expression vector for HPr	Seok <i>et al.</i> (1997)
pSP100(L47A/F48A)	pRE1-based expression vector for HPr(L47A/F48A)	This study
pPR6	pRE1-based expression vector for EI	Seok <i>et al.</i> (1996)
pETDuet-1	Expression vector under control of T7 promoter/ <i>lac</i> operator, Amp ^r	Novagen
pET-HisRsd	Expression vector for Rsd with His tag	Park <i>et al.</i> (2013)
pET-HisRsd(E51R)	Expression vector for Rsd(E51R) with His tag	This study
pET-HisRsd(C58D)	Expression vector for Rsd(C58D) with His tag	This study
pET-HisRsd(Y107A)	Expression vector for Rsd(Y107A) with His tag	This study
pET-HisRpoD	Expression vector for σ ⁷⁰ with His tag	Park <i>et al.</i> (2013)
pACYC-184	Cloning vector; Cm ^r Tet ^r	Chang & Cohen (1978)
pACYC-Rsd	<i>E. coli</i> <i>rsd</i> gene and its promoter cloned between BamHI and SphI sites of pACYC-184	Park <i>et al.</i> (2013)
pACYC-Rsd-H15A	<i>E. coli</i> mutated <i>ptsH</i> gene and its promoter cloned between SphI and SalI sites of pACYC-Rsd	Park <i>et al.</i> (2013)
pACYC-Rsd(E51R)	Rsd(E51R) mutation by QuikChange PCR using mutagenic primers and pACYC-Rsd as a template	This study
pACYC-Rsd(C58D)	Rsd(C58D) mutation by QuikChange PCR using mutagenic primers and pACYC-Rsd as a template	This study
pACYC-Rsd(Y107A)	Rsd(Y107A) mutation by QuikChange PCR using mutagenic primers and pACYC-Rsd as a template	This study
pACYC-Rsd(E51R)-H15A	Rsd(E51R) mutation by QuikChange PCR using mutagenic primers and pACYC-Rsd-H15A as a template	This study
pACYC-Rsd-H15A(L47A/F48A)	HPr(L47A/F48A) mutation by QuikChange PCR using mutagenic primers and pACYC-Rsd-H15A as a template	This study

forms of PTS components increases owing to rapid transfer of the phosphoryl group to incoming sugar molecules, whereas phosphorylation increases in the absence of PTS sugars (Deutscher *et al.*, 2014). In this way, the PTS can sense nutritional changes in the environment and regulate a variety of metabolic processes. For example, dephosphorylated EI inhibits the autophosphorylation of CheA in the presence of glucose to regulate chemotaxis towards sugar (Lux *et al.*, 1995). EIIA^{Glc} is a key player in carbon-catabolite repression (Deutscher *et al.*, 2014). The dephosphorylated form of EIIA^{Glc} inhibits several non-PTS sugar permeases as well as glycerol kinase for preferential utilization of PTS sugars over non-PTS sugars. Phosphorylated EIIA^{Glc} activates adenyl cyclase to induce the expression of many metabolic enzymes for non-PTS sugars in the absence of PTS sugars (Park *et al.*, 2006). EIIA^{Glc} also regulates the fermentation/respiration switch protein FrsA (Koo *et al.*, 2004). Dephosphorylated EIICB^{Glc} sequesters the global repressor Mlc to the membrane to induce the expression of several PTS components in the presence of PTS sugars (Nam *et al.*, 2008). Dephosphorylated HPr also activates glycogen phosphorylase to regulate carbon storage (Seok *et al.*, 1997).

A recent ligand-screening experiment with HPr revealed that only the unphosphorylated form of HPr has a strong affinity towards Rsd in *Escherichia coli* (Park *et al.*, 2013). Rsd is more highly expressed in stationary-phase cells than in exponentially growing cells and functions as an anti-sigma factor to sequester the housekeeping sigma factor σ⁷⁰ (Jishage & Ishihama, 1998; Piper *et al.*, 2009). HPr mainly exists in its

dephosphorylated form in the presence of PTS sugars. The binding of dephosphorylated HPr to Rsd antagonizes the function of Rsd by sequestering Rsd from σ⁷⁰, allowing σ⁷⁰ to bind to core RNA polymerase to express housekeeping genes. When the PTS sugar is completely used, however, HPr becomes phosphorylated. Because phosphorylated HPr cannot antagonize Rsd, Rsd facilitates switching of the sigma subunit on RNA polymerase from σ⁷⁰ to σ^S and probably other sigma factors. Under these conditions, cells can express stationary-phase genes and stress-responsive genes (Park *et al.*, 2013).

To date, the structure of the Rsd-σ⁷⁰ complex (Westblade *et al.*, 2004; Patikoglou *et al.*, 2007) and many HPr structures (Garrett *et al.*, 1999; Jung *et al.*, 2012; Herzberg *et al.*, 1992) have been solved. However, the binding interface between HPr and Rsd has not yet been described. In this study, the crystal structure of the *E. coli* HPr-Rsd complex has been determined at 2.1 Å resolution. The results provide a structural basis for the sequestration of Rsd from σ⁷⁰ by HPr in response to nutrient availability in the external environment.

2. Methods and materials

2.1. Plasmid construction and protein purification

Purification of EI and HPr was accomplished as described previously (Seok *et al.*, 1997; Koo *et al.*, 2004), and Rsd and σ⁷⁰ were purified in a similar manner (Park *et al.*, 2013). To purify the hexahistidine-tagged protein complex, cells over-

Table 2
Mutagenic primers for site-directed mutagenesis in Rsd and HPr.

Mutation	Mutagenic primers
Rsd	
E51R	5'-TACATGAGGCTAAACAGAAAAGCCCTTGATGATTTTTGTC-3' 5'-GACAAAAATCATCAAGGGCTTTTCTGTTTAGCCTCATGTA-3'
C58D	5'-GATTTTGACCAGAGCCTGGTCGATTACTTGTCTGC-3' 5'-GCAGACAAGTAATCGACCAGGCTCTGGTCAAAAATC-3'
Y107A	5'-CAACAGATTATGGATTACGCAGATTCCAGTCTGGAAACCG-3' 5'-CGGTTTCAGACTGGAATCTGCGTAATCCATAATCTGTTG-3'
HPr	
L47A/F48A	5'-GCGCCAGCGGAAAAGCGCGGCGAAACTGCAGACTCTGGGCCT-3' 5'-AGGCCAGAGTCTGCAGTTTCGCTGCGCTTTTCGCGCTGGCGC-3'

Table 3
Data-collection and refinement statistics for the Rsd–HPr complex.

Values in parentheses are for the highest resolution shell.

Wavelength (Å)	0.979
Resolution limit (Å)	29.6–2.1 (2.17–2.10)
Space group	$P3_221$
Unit-cell parameters (Å)	$a = 74.8, b = 74.8, c = 72.7$
Unique reflections	13804 (1359)
Multiplicity	15.8 (7.2)
R_{merge} (%)	7.0 (37.0)
Completeness (%)	97.1 (97.4)
$CC_{1/2}$	0.999 (0.957)
Average $I/\sigma(I)$	44.4 (7.5)
Refinement	
Resolution range (Å)	29.6–2.1 (2.17–2.10)
R factor (%)	21.8 (30.3)
$R_{\text{free}}^{\dagger}$ (%)	29.8 (30.8)
No. of protein atoms	1851
No. of water molecules	28
Average B value, protein atoms (Å ²)	38.3
Average B value, water molecules (Å ²)	34.9
Wilson B value (Å ²)	31.7
R.m.s.d., bonds (Å)	0.019
R.m.s.d., angles (°)	1.84
Ramachandran plot	
Most favoured	94.8
Additionally favoured	0.4
Coordinate error (Å)	0.36
PDB code	4xwj

[†] R_{free} was calculated with 5% of the data set.

expressing the protein complex were resuspended in 20 mM Tris pH 8.0 buffer containing 150 mM NaCl and 2 mM β -mercaptoethanol. After disruption by sonication at 277 K, the insoluble fraction was removed by centrifugation at 19 000g for 0.5 h. The protein was initially purified by Ni–NTA affinity chromatography at 277 K. The resin was washed with ten column volumes of 20 mM Tris pH 8.0 buffer containing 150 mM NaCl, 20 mM imidazole and 2 mM β -mercaptoethanol. The protein complex was eluted with four column volumes of 20 mM Tris pH 8.0 buffer containing 150 mM NaCl, 250 mM imidazole and 2 mM β -mercaptoethanol. The protein complex was applied onto a HiLoad Superdex 16/60 200 column (GE Healthcare, USA) pre-equilibrated with ten column volumes of 20 mM Tris pH 8.0 buffer containing 150 mM NaCl and 2 mM β -mercaptoethanol at 295 K. The purified protein complex was concentrated to 10 mg ml^{−1} using Centriprep centrifugal filter devices (Millipore, USA) at 277 K and stored frozen at 193 K until use. The protein

concentration was determined by measuring the absorbance at 280 nm based on the molar extinction coefficient (20 065 M^{−1} cm^{−1}). For the purification of σ^{70} , 10% glycerol was added to the buffer. All strains and plasmids used in this study are listed in Table 1.

2.2. Site-directed mutagenesis of Rsd and HPr

To create amino-acid substitution mutations, the QuikChange protocol was used (Braman *et al.*, 1996). The primers used to introduce point mutations in Rsd and HPr are listed in Table 2. The respective plasmids used as templates with these primers are pET–HisRsd (Park *et al.*, 2013), pSP100 (Seok *et al.*, 1997), pACYC–Rsd and pACYC–Rsd–H15A (Park *et al.*, 2013). These mutagenic primers were used to amplify DNAs using the high-fidelity DNA polymerase *n*Pfu Forte (Enzymomics). All clones were sequenced to confirm that the mutations had been successfully introduced. The mutated proteins were expressed and purified in the same manner as the wild-type proteins.

2.3. Crystallization and structural determination

One rod-shaped crystal was obtained by vapour diffusion using a sitting-drop setup in 96-well plates and a sparse-matrix screen (Hampton Research) at 287 K. This was performed by mixing 0.5 μ l protein solution (10 mg ml^{−1}) with 0.5 μ l well solution (0.1 M NaCl, 0.1 M HEPES pH 7.5, 1.6 M ammonium sulfate) and equilibrating against 60 μ l well solution. The crystal from the initial crystallization trial was used to collect X-ray diffraction data on beamline 5C of the Pohang Accelerator Laboratory (PAL), Republic of Korea using a Quantum 270 CCD detector (ADSC). The diffraction data set was processed and scaled to 2.1 Å resolution with the *HKL*-2000 package (Otwinowski & Minor, 1997). A non-optimal camera geometry resulted in the collection of data to a resolution that was lower than the diffraction limit of the crystal. Unfortunately, subsequent crystals did not diffract as well. The crystal belonged to space group $P3_221$, with unit-cell parameters $a = b = 74.8, c = 72.7$ Å.

The initial phases were determined by the molecular-replacement method using the coordinates of Rsd in the Rsd– σ^{70} domain 4 complex (PDB entry 2p7v; Patikoglou *et al.*, 2007) and HPr from *E. coli* (PDB entry 1cm3; Napper *et al.*, 1999) as search models with *MOLREP* (Vagin & Teplyakov, 2010) from the *CCP4* suite (Winn *et al.*, 2011). Model building was performed using *Coot* (Debrecezeni & Emsley, 2012) and refinement was carried out using *PHENIX* (Adams *et al.*, 2002). Crystallographic data statistics are summarized in Table 3. A random set of 5% of the reflections was excluded from the refinement for cross-validation of refinement strategies. Water molecules were assigned automatically for peaks of $>2\sigma$ in the $F_o - F_c$ difference maps by cycling refinement using *PHENIX* (Adams *et al.*, 2002), and some were deleted

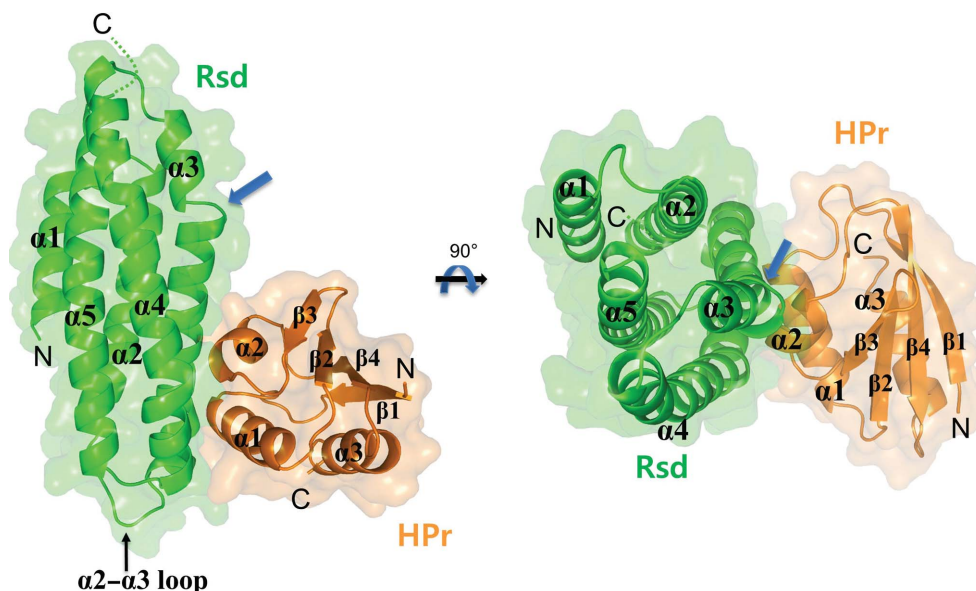


Figure 1
Structure of the Rsd–HPr complex. Ribbon diagrams showing two orthogonal views of the complex. Semi-transparent surface representations are overlaid on the ribbon diagrams. Rsd is shown in green and HPr is shown in orange. The kink in Rsd at $\alpha 3$ is indicated by blue arrows. The loop connecting $\alpha 2$ and $\alpha 3$ is labelled and is indicated by a black arrow. Secondary-structural elements are labelled.

by manual inspection. The model quality was verified using *MolProbity* (Chen *et al.*, 2010). All residues were in the favoured region of the Ramachandran plot. Detailed statistics for X-ray data collection and refinement are presented in Table 3. The coordinates and structure factors have been deposited in the Protein Data Bank (PDB entry 4xwj). Figures were generated using *PyMOL* (DeLano, 2002).

2.4. Co-purification experiments employing metal-affinity chromatography

80 μg of wild-type and site-directed mutant forms of His-Rsd were mixed with 40 μg wild-type HPr or HPr(L47A/F48A). Each mixture was then incubated with 30 μl BD TALON metal-affinity resin in a 1.7 ml tube for 10 min to undergo metal-affinity chromatography. After briefly washing with buffer containing 10 mM imidazole, the proteins bound to the resin were eluted with 2 \times SDS loading buffer. To analyze complex formation between His-Rsd and HPr, the eluted proteins were run on SDS–PAGE and stained with Coomassie Brilliant Blue R.

2.5. RNA isolation and qRT-PCR

Total RNA was prepared using an RNeasy Mini kit (Qiagen) from cells grown to stationary phase in LB medium containing 20 $\mu\text{g ml}^{-1}$ chloramphenicol, and DNA was removed using RNase-free DNase (New England Biolabs). The total RNA from each culture (2.5 μg) was converted to cDNA using cDNA EcoDry Premix (Clontech). The cDNAs were diluted tenfold and subjected to qRT-PCR analyses using gene-specific primers and SYBR Premix Ex Taq II (Takara). The amplification and detection of specific products were performed using a CFX96TM Real-Time System (Bio-Rad).

For normalization of the transcription level, the *rrsG* gene was used as a reference. The relative expression level was calculated as the difference between the threshold cycle (Ct) of the target gene and the Ct of the reference gene for each template.

2.6. Measurement of binding affinity monitored by surface plasmon resonance (SPR)

The real-time interaction of Rsd variants with HPr was monitored by SPR detection using a BIAcore 3000 system (GE Healthcare Life Sciences) as described previously, with some modifications (Lee *et al.*, 2007, 2010). Each Rsd variant was immobilized onto the carboxy-methylated dextran surface of a CM5 sensor chip. Each Rsd variant (100 μl , 20 $\mu\text{g ml}^{-1}$) in

coupling buffer (20 mM sodium acetate pH 4.6) was flowed over the sensor chip at 5 $\mu\text{l min}^{-1}$ to couple the proteins to the matrix by an *N*-hydroxysuccinimide/*N*-ethyl-*N'*-(3-diethylaminopropyl)carbodiimide (NHS/EDC) reaction (80 μl mixture). Assuming that 1000 resonance units correspond to a surface concentration of 1 ng mm^{-2} , each Rsd variant was immobilized to a surface concentration of 1–1.2 ng mm^{-2} . The standard running buffer was 20 mM HEPES–NaOH pH 7.5, 150 mM NaCl, and all reagents were introduced at a flow rate of 10 $\mu\text{l min}^{-1}$. Four different concentrations (0.25, 0.5, 1 and 2 μM) of HPr were applied to the Rsd-bound sensor chip. The sensor surface was regenerated between assays by using the standard running buffer at a flow rate of 100 $\mu\text{l min}^{-1}$ for 10 min to remove bound analytes. Kinetics parameters for the interaction of HPr with immobilized Rsd variants were determined using the *BIAevaluation* 2.1 software (GE Healthcare Life Sciences).

3. Results

3.1. Overall structure of the HPr–Rsd complex

The crystals contained one HPr–Rsd complex in the asymmetric unit, with a solvent content of 35%. The structure of the complex was determined by the molecular-replacement method using the structures of HPr and Rsd as search models. The final model was refined to an R_{work} and R_{free} of 21.8 and 29.8%, respectively, at 2.1 Å resolution. The structure revealed a 1:1 complex of HPr and Rsd, consistent with previous results from size-exclusion chromatography (Park *et al.*, 2013). The overall structure of the complex resembles the letter L. The smaller globular HPr is bound to the lower region of the rod-shaped Rsd structure (Fig. 1).

3.2. Rsd and HPr structure

The structure of Rsd in the HPr–Rsd complex is similar to the structure of Rsd in the Rsd– σ^{70} complex (Westblade *et al.*, 2004; Fig. 2*a*). The Rsd structure consists of four core α -helical bundles ($\alpha 2$ – $\alpha 5$) packed up and down with a slight left-handed twist. An additional shorter N-terminal α -helix ($\alpha 1$) is attached to the interhelical space between $\alpha 2$ and $\alpha 5$ in the four core α -helical bundles. Superposition of the Rsd structures in the HPr–Rsd and Rsd– σ^{70} complexes yields an r.m.s.d. of 0.492 Å over 122 C α atoms. A pronounced kink ($\sim 30^\circ$) in $\alpha 3$ at the highly conserved residues Gly68, His69 and Phe70 is also found in the Rsd complex with HPr, as observed in the Rsd– σ^{70} complex structure (Westblade *et al.*, 2004; Fig. 1). Conformational variations were only found in the loops connecting α -helices and are likely to be the result of differences in crystal packing. All residues of Rsd are ordered except for the C-terminal seven residues in the crystal structure of the HPr–Rsd complex. The loop connecting $\alpha 2$ and $\alpha 3$ is disordered in the Rsd– σ^{70} structure.

NMR and X-ray crystallography have been used to determine the structures of HPr alone and in complex with EII or EI (El-Kabbani *et al.*, 1987; Herzberg *et al.*, 1992; Jung *et al.*, 2012; Garrett *et al.*, 1999; Jia *et al.*, 1993). HPr is a small rigid protein (~ 9 kDa) consisting of four antiparallel β -strands and three α -helices with a $\beta\alpha\beta\beta\alpha\beta\alpha$ folding pattern (Jia *et al.*, 1994). The structural variation in HPrs from Gram-positive and Gram-negative bacteria is very limited. Only the N- and C-terminal residues exhibited different conformations. The principal active-site residue His15 accepts and donates a phosphoryl group in the phosphoryl-transfer cascade (Weigel *et al.*, 1982; Deutscher *et al.*, 2014). His15 is located in a solvent-exposed area of the N-caps of the α -helix ($\alpha 1$). Phosphorylation at His15 of HPr does not induce a substantial structural change (Jia *et al.*, 1994). Structural superposition revealed that the structure of HPr in complex with Rsd is similar to that of HPr in complex with EI or EII, yielding an r.m.s.d. of 0.779 Å with HPr–EI between 82 C α atoms (Garrett *et al.*, 1999) and an r.m.s.d. of 0.384 Å with HPr–EII^{chitobiose} between 72 C α atoms (Figs. 2*b* and 2*c*).

3.3. Binding interface of Rsd with HPr

Given the low K_d value (~ 8.9 nM) for HPr and Rsd, which is comparable to that for Rsd and σ^{70} (~ 30 nM), the protein–protein interaction of the two proteins appears to be stable (Park *et al.*, 2013; Sharma & Chatterji, 2008). The complex structure has a buried surface area on binding of HPr to Rsd of 1715 Å², which is not as large as the total solvent-accessible surface area of Rsd (9250 Å²). The binding interface is formed by the lower part of the surfaces of $\alpha 3$ and $\alpha 4$ of the Rsd α -helical bundle and $\alpha 1$ and $\alpha 2$ of HPr (Fig. 1). The interactions are focused in a small area and include both polar and hydrophobic interactions (Fig. 3).

Along with the carbonyl group of Gln51, the backbone amide and hydroxyl groups of Thr16 from HPr create a hydrogen-bonding network with the side chains of Asp55, Gln59 and Tyr107 from Rsd (Figs. 3*a* and 3*b*). Glu51 of Rsd

forms an ionic interaction with Arg17 of HPr and forms a water-mediated hydrogen bond with His15 from HPr. Glu112 of Rsd interacts ionically with Lys27 and the backbone amide group of Leu47 from HPr. Likewise, Asp116 of Rsd makes polar interactions with Lys24 of HPr. Asp108 of Rsd forms a hydrogen-bonding network with the backbone amide groups of Leu47 and Phe48 and the side chain of Ser46 from HPr. Phe48 of HPr is a key residue for hydrophobic interaction with Rsd. HPr Phe48 is located in the groove between $\alpha 3$ and $\alpha 4$ of the Rsd α -helical bundle, forming van der Waals contacts with Val62, Leu65, Met104 and Tyr107 of Rsd (Figs. 3*a* and 3*b*). Tyr107 of Rsd is also involved in hydrophobic contacts with Leu47 and Phe48 of HPr (Figs. 3*a* and 3*b*).

To validate the significance of the newly identified residues at the interface for the formation of a stable complex, alanine substitutions were generated at Leu47 and Phe48 of HPr. These residues are involved in hydrophobic interactions with Tyr107 of Rsd. When HPr is phosphorylated by EI, the phosphorylated form of HPr runs faster than the dephosphorylated form on a nondenaturing polyacrylamide gel

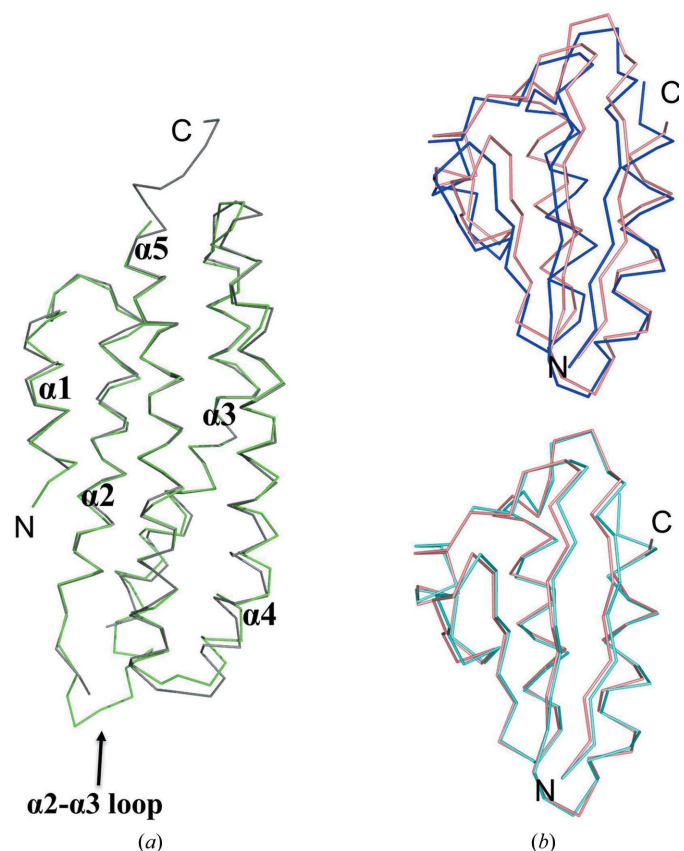


Figure 2
Structural comparison of Rsd and HPr. (a) Structural superposition of Rsd (green) in complex with HPr and Rsd (grey) in complex with σ^{70} (PDB entry 2p7v; Patikoglou *et al.*, 2007). (b) Structural comparison of HPr structures when complexed with Rsd, EI and EII. Top, superposition of the HPr structure in the HPr–Rsd complex (pink) with that in the HPr–EI complex (PDB entry 1zym; blue; Liao *et al.*, 1996). Bottom, superposition of the HPr structure in the HPr–Rsd complex (pink) with that in the HPr–EIIA^{chitobiose} complex (PDB entry 2lrk; cyan; Jung *et al.*, 2012).

(compare lanes 2 and 3 in Fig. 4*a*; Park *et al.*, 2013). The site-directed variant of HPr, HPr(L47A/F48A), was readily phosphorylated by EI as efficiently as wild-type HPr *in vitro* (Fig. 4*a*). These results indicate that HPr(L47A/F48A) is folded correctly and interacts functionally with EI. To investigate the importance of Leu47 and Phe48 of HPr in complex formation with Rsd, purified Rsd protein containing a hexahistidine tag (His-Rsd) was mixed with wild-type HPr or the HPr(L47A/F48A) variant and subjected to Talon metal-affinity chromatography (Fig. 4*b*). As expected from the crystal structure (Figs. 3*a* and 3*b*), substitution of Leu47 and

Phe48 with Ala abrogated the co-precipitation of HPr with His-Rsd (compare lanes 2 and 5 in Fig. 4*b*), while wild-type HPr formed a stable complex with His-Rsd (compare lanes 1 and 4 in Fig. 4*b*). These results confirm the validity of the complex model for Rsd and HPr.

To investigate whether mutations of Rsd-binding residues (Leu48 and Phe48) affect the regulatory function of HPr as an anti-Rsd factor or a σ^S -stimulating factor, the expression levels of Rsd-dependent genes in *E. coli* were compared. As observed previously (Mitchell *et al.*, 2007; Park *et al.*, 2013), the expression levels of the σ^S -dependent genes *hdeA* and *gadA* decreased significantly in the *rsd* deletion mutant, while their expression levels were restored by exogenous expression of Rsd. The stimulatory effect of Rsd on *hdeA* and *gadA* expression was completely antagonized when Rsd was co-expressed with HPr(H15A), a nonphosphorylatable form of HPr. However, HPr(H15A) containing the additional mutations L47A and F48A did not antagonize the stimulatory effect of Rsd on the expression of σ^S -dependent genes (Fig. 4*c*). These results indicate that hydrophobic interactions of Rsd with HPr through Leu47 and Phe48 are important in compromising the ability of Rsd to sequester σ^{70} from the core RNA polymerase and to increase the RNA polymerase containing σ^S .

Binding between Rsd and HPr is abolished when His15 of HPr is phosphorylated, such as in the absence of glucose. His15 in HPr is positioned in the binding interface of Rsd and HPr, between the carboxylic groups of Asp55 and Glu51 of Rsd (Fig. 3). When His15 of HPr is phosphorylated *in silico*, the bulkier residue is likely to cause severe steric hindrance at the binding interface, as well as charge repulsion with Asp55 and/or Glu51 of Rsd (Fig. 3*c*). To verify the electrostatic and steric hindrance imposed by these amino-acid residues, Glu51 of Rsd was substituted by the positively charged amino acid Arg. Rsd-HPr complex formation was then examined using electrophoretic mobility shift assays.

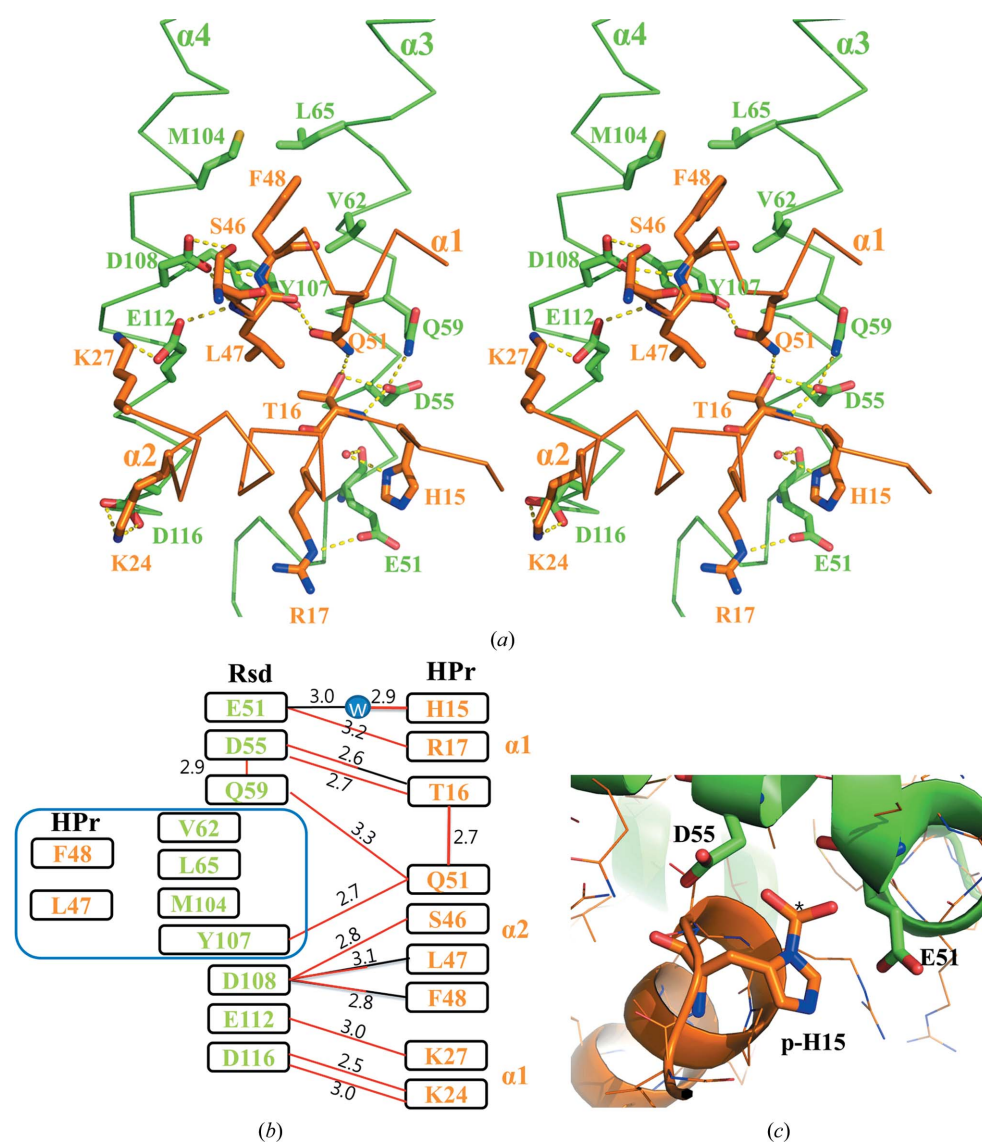


Figure 3

Binding interface between Rsd and HPr. (a) Stereoview of the HPr-Rsd interface. Protein C α backbone traces are colour-coded as in Fig. 1. Amino-acid side chains or backbone atoms that participate in interprotein interactions are shown in stick representation with the same C-atom colours as the C α trace. N atoms are blue and O atoms are red. Broken yellow lines indicate interprotein polar interactions. (b) Schematic diagram denoting molecular interactions between Rsd and HPr. Hydrophobic interactions are shown on the left (blue box). Polar interactions (hydrogen bonds and ionic interactions) are shown on the right. Backbone-mediated interactions are indicated by black lines and side-chain-mediated interactions are indicated by red lines. 'w' denotes a water molecule. Residues involved in hydrophobic interactions are shown in a blue box. The distances (\AA) of the polar interactions are indicated. (c) Structure focusing on His15 of HPr. A phosphoryl group is modelled at His15 and is denoted by an asterisk.

When a mixture of HPr and wild-type Rsd was subjected to native PAGE, a new band representing the Rsd–HPr complex appeared between the Rsd and HPr bands, with a concomitant decrease in the intensity of the Rsd and HPr bands (Fig. 5a). When the E51R variant of Rsd was mixed with HPr, the decreased intensity of the HPr band was less evident, even though the Rsd mobility was slightly shifted (compare the bands marked with red arrowheads in Fig. 5a). To quantify the

effect of the E51R mutation of Rsd on HPr, we carried out Biacore/SPR experiments to determine the binding constant. As shown in Table 4, the E51R mutation in Rsd decreased the affinity for HPr by ~100-fold. These data demonstrate that Rsd(E51R) interacts with HPr with a weaker affinity than wild-type Rsd. The weaker interaction between Rsd(E51R) and HPr was confirmed by Talon metal-affinity chromatography. When the same amount of HPr was mixed with

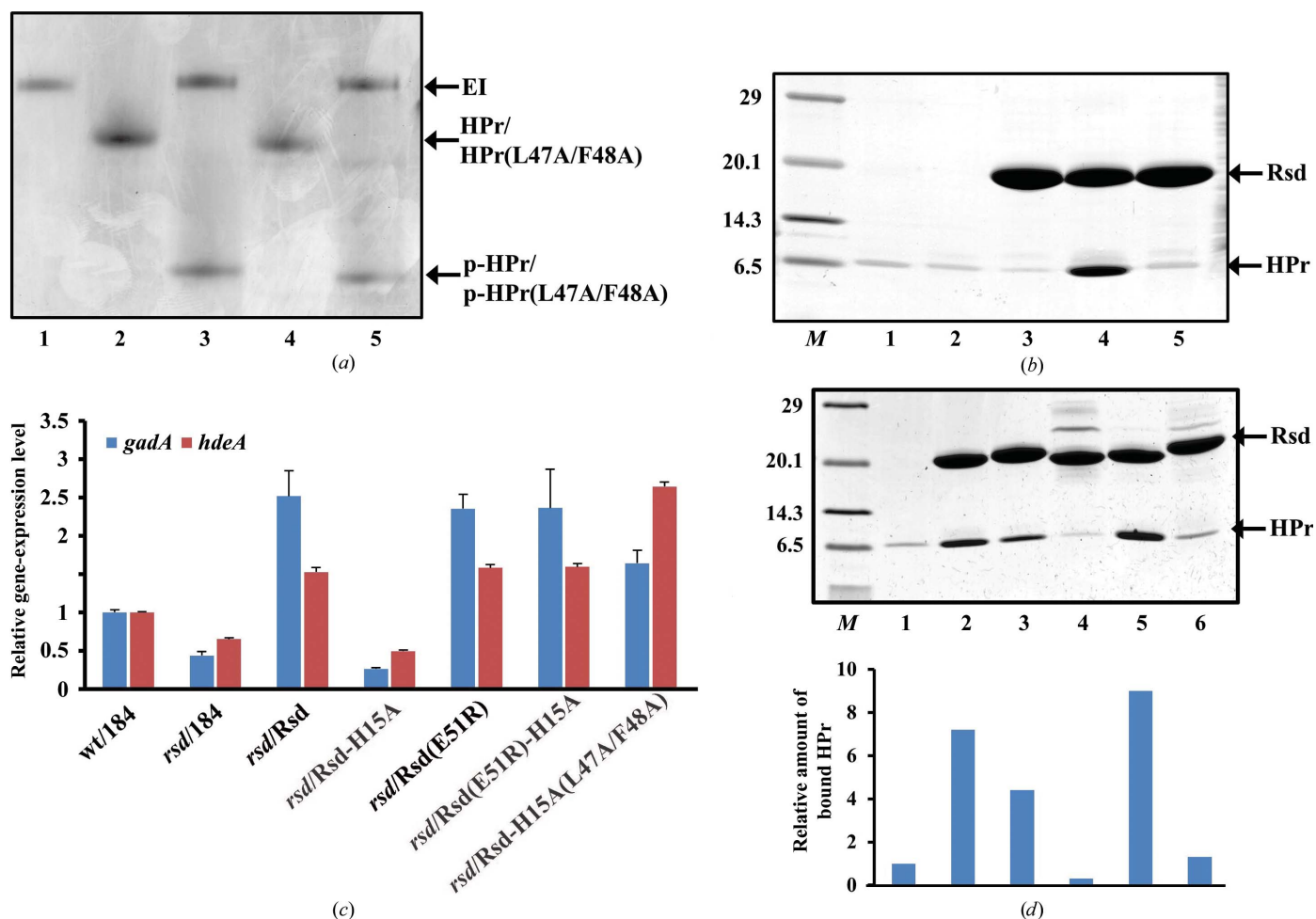


Figure 4 Biochemical analyses based on the structure of the complex. (a) Phosphorylation of the site-directed mutant HPr(L47A/F48A). To test whether HPr(L47A/F48A) could be phosphorylated by EI and PEP like wild-type HPr, EI and HPr or HPr(L47A/F48A) were incubated in 20 mM HEPES–NaOH pH 7.5 containing 100 mM NaCl, 2 mM MgCl₂, 2 mM PEP at 37°C for 10 min. Each sample was analyzed by native PAGE to measure the electrophoretic mobility shift of the phosphorylated form of HPr. Lane 1, 1 µg EI; lane 2, 2.5 µg HPr; lane 3, 1 µg EI and 2.5 µg HPr; lane 4, 2.5 µg HPr(L47A/F48A); lane 5, 1 µg EI and 2.5 µg HPr(L47A/F48A). (b) Importance of the Leu47 and Phe48 residues of HPr in binding to Rsd. His-Rsd (80 µg) was mixed with wild-type HPr or HPr(L47A/F48A) (40 µg each) and subjected to Talon resin for metal-affinity chromatography. After brief washing, the proteins bound to the resin were eluted with 2× SDS loading buffer. Complex formation was analyzed by SDS–PAGE and staining with Coomassie Brilliant Blue R. Lane M, molecular-mass markers (KOMA Biotech; labelled in kDa); lane 1, HPr alone; lane 2, HPr(L47A/F48A) alone; lane 3, His-Rsd alone; lane 4, His-Rsd and HPr; lane 5, His-Rsd and HPr(L47A/F48A). (c) Effect of HPr or Rsd mutations on transcription from σ^S -dependent promoters *in vivo*. Total RNA was isolated from the indicated *E. coli* strains grown to stationary phase in LB medium. *gadA* (blue bars) and *hdeA* (red bars) mRNA levels were then measured by qRT-PCR. Representative data (means \pm SDs) from two independent experiments ($n = 3$ each) are shown. The strains used are the wild type (wt) and an *rsd* deletion mutant (*rsd*) harbouring pACYC184 (184; control vector), pACYC-Rsd (Rsd expression vector), pACYC-Rsd(E51R) [Rsd(E51R) expression vector], pACYC-Rsd-H15A [plasmid co-expressing both Rsd and HPr(H15A)] or pACYC-Rsd-H15A(L47A/F48A) [plasmid co-expressing both Rsd and HPr(H15A/L47A/F48A)] as indicated (see Table 1 for strains and plasmids). (d) Analysis of the interaction between HPr and mutated forms of Rsd by metal-affinity chromatography. Wild-type and site-directed mutants of His-Rsd (80 µg each) were mixed with HPr (40 µg) and 30 µl Talon resin for metal-affinity chromatography. After a brief wash, the proteins bound to the resin were eluted with 2× SDS loading buffer. To analyze complex formation between His-Rsd and HPr, the eluted proteins were run on SDS–PAGE and stained with Coomassie Brilliant Blue R. Protein levels of HPr were quantified using the *Multi Gauge* software (Fuji) and are indicated as a histogram below the gel. Lane M, molecular-mass markers (KOMA Biotech Inc.); lane 1, HPr; lane 2, His-Rsd and HPr; lane 3, His-Rsd(E51R) and HPr; lane 4, His-Rsd(C58D) and HPr; lane 5, His-Rsd(C58S) and HPr; lane 6, His-Rsd(Y107A) and HPr.

Table 4
Measurement of the dissociation constant (K_d) between Rsd variants and HPr.

Each purified Rsd variant was separately immobilized onto the carboxy-methylated dextran surface of a CM5 sensor chip using an NHS/EDC reaction and the real-time interaction of HPr with Rsd was monitored by SPR detection using a Biacore 3000 system (GE Healthcare Life Sciences) as described previously (Lee *et al.*, 2007, 2010). Various amounts of HPr were allowed to flow over the Rsd surface at a flow rate of $10 \mu\text{l min}^{-1}$ for 90 s. The sensor surface was regenerated between assays by injecting the standard running buffer at a flow rate of $100 \mu\text{l min}^{-1}$ for 10 min to remove bound analytes. The K_d value was determined using the *BIAevaluation* 2.1 software (GE Healthcare Life Sciences). Data are the mean \pm standard deviation ($n = 3$).

Rsd variant	K_d (M)
Wild type	$4.45 \times 10^{-9} \pm 3.52 \times 10^{-9}$
E51R	$1.88 \times 10^{-6} \pm 2.74 \times 10^{-6}$
Y107A	ND

His-tagged forms of wild-type Rsd and Rsd(E51R), the amount of HPr pulled down by Rsd(E51R) was significantly less than that pulled down by wild-type Rsd (Fig. 4d).

However, the E51R mutation did not affect the complex formation of Rsd with σ^{70} (Fig. 5b). While HPr sequestered wild-type Rsd from σ^{70} to form the Rsd–HPr complex (Fig. 5c, top, fourth lane), it could not sequester Rsd(E51R) from σ^{70} when it was added to a mixture containing Rsd(E51R) and σ^{70} (Fig. 5c, top, sixth lane). This result also confirms the weaker interaction of Rsd(E51R) with HPr compared with wild-type Rsd.

3.4. Functional analysis

The *in vivo* effect of the weaker interaction between Rsd(E51R) and HPr was examined by determining the expression levels of the σ^S -dependent genes *hdeA* and *gadA* (Fig. 4c). The exogenous expression of Rsd(E51R) stimulated the expression of these genes as efficiently as wild-type Rsd in the *rsd* deletion strain. While HPr(H15A) antagonized the stimulatory effect of wild-type Rsd on the expression of these genes, it did not antagonize the effect of Rsd(E51R). These

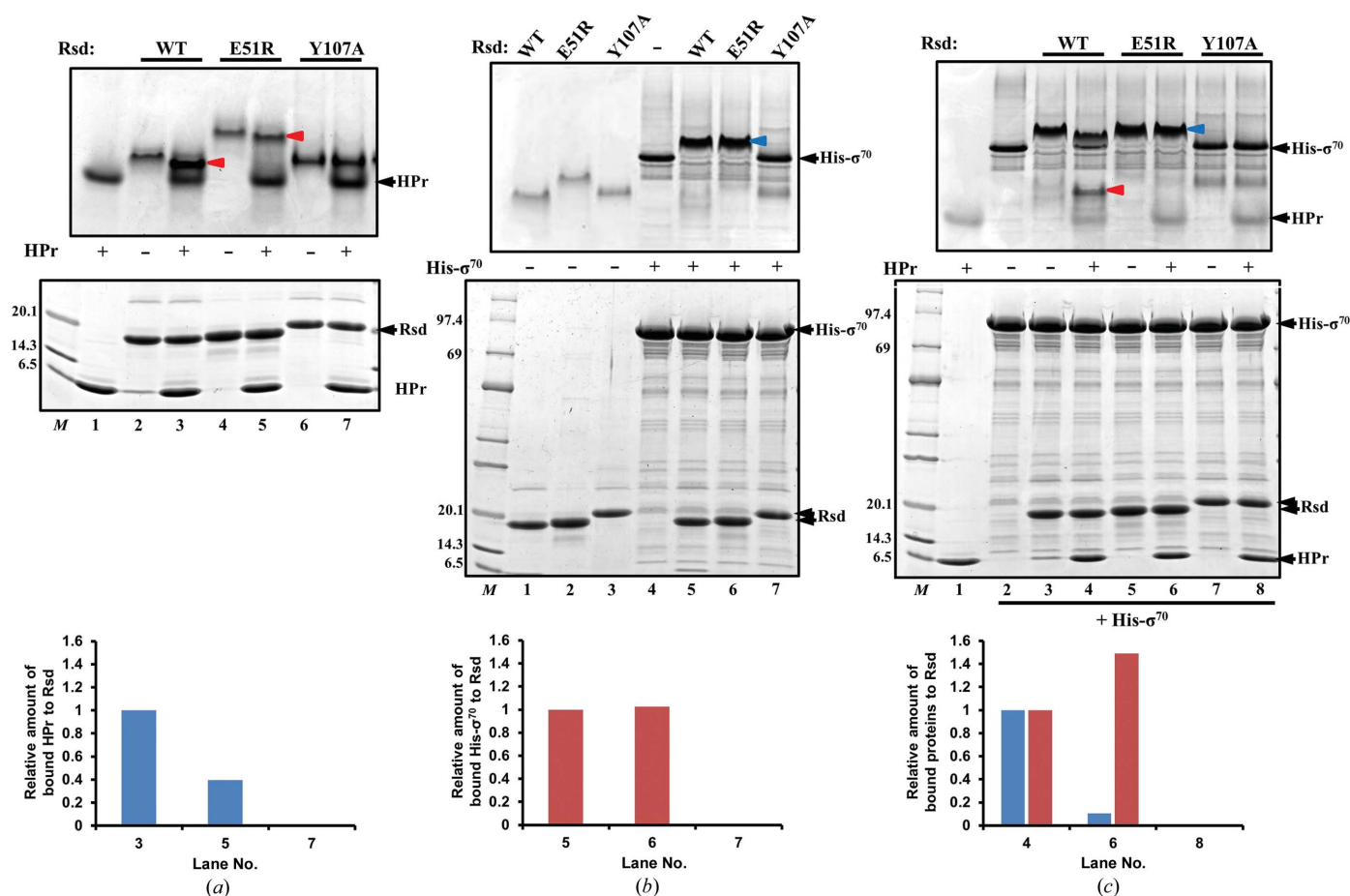


Figure 5
Electrophoretic mobility shift of Rsd with σ^{70} and HPr on a native gel. The effects of amino-acid substitutions of Rsd on complex formation with HPr (a) and σ^{70} (b) and on competition between σ^{70} and HPr for binding to Rsd (c) were tested. HPr [3 μg in (a) and 0.8 μg in (c)] and σ^{70} (9 μg) were incubated with wild-type or mutant forms of Rsd (2 μg) in different combinations, as indicated, in 20 mM HEPES–NaOH pH 7.5 containing 100 mM NaCl at 37°C for 10 min. Complex formation was confirmed by nondenaturing PAGE (upper gels), and the amounts of the proteins by SDS–PAGE (lower gels). The histograms below the SDS–PAGE gels indicate the relative amounts of proteins (blue bars, HPr; red bars, σ^{70}) complexed with Rsd. The relative band intensities were quantified using the *Multi Gauge* software (Fuji). Blue arrows, complex between His-Rsd and σ^{70} ; red arrows, complex between His-Rsd and HPr.

results explain the phosphorylation-dependent regulation of protein–protein interaction.

3.5. Comparison of the binding interface of Rsd–HPr with that of Rsd– σ^{70}

To gain insight into how HPr antagonizes the function of Rsd in sequestering σ^{70} , the binding interfaces of Rsd–HPr and Rsd– σ^{70} were compared. The buried surface area between Rsd and HPr (1715 Å²) is slightly larger than that of Rsd and σ^{70} (1492 Å²). Consistently, the K_d value of HPr for Rsd is

also comparable to that of σ^{70} for Rsd (Park *et al.*, 2013). The molecular size of domain 4 of σ^{70} , which is responsible for the recognition of Rsd and the promoter region, is ~8 kDa and is similar to that of HPr (~9 kDa). However, the binding region on Rsd is distinct despite an overlapping region on Rsd (Fig. 6*a*). The surface formed with $\alpha 3$ and $\alpha 4$ in the helical bundle of Rsd shares a binding surface with HPr and σ^{70} . However, HPr is exclusively bound to the lower part of the $\alpha 3$ – $\alpha 4$ surface of Rsd, while domain 4 of σ^{70} mainly occupies the central part of the Rsd surface. Domain 4 of σ^{70} makes

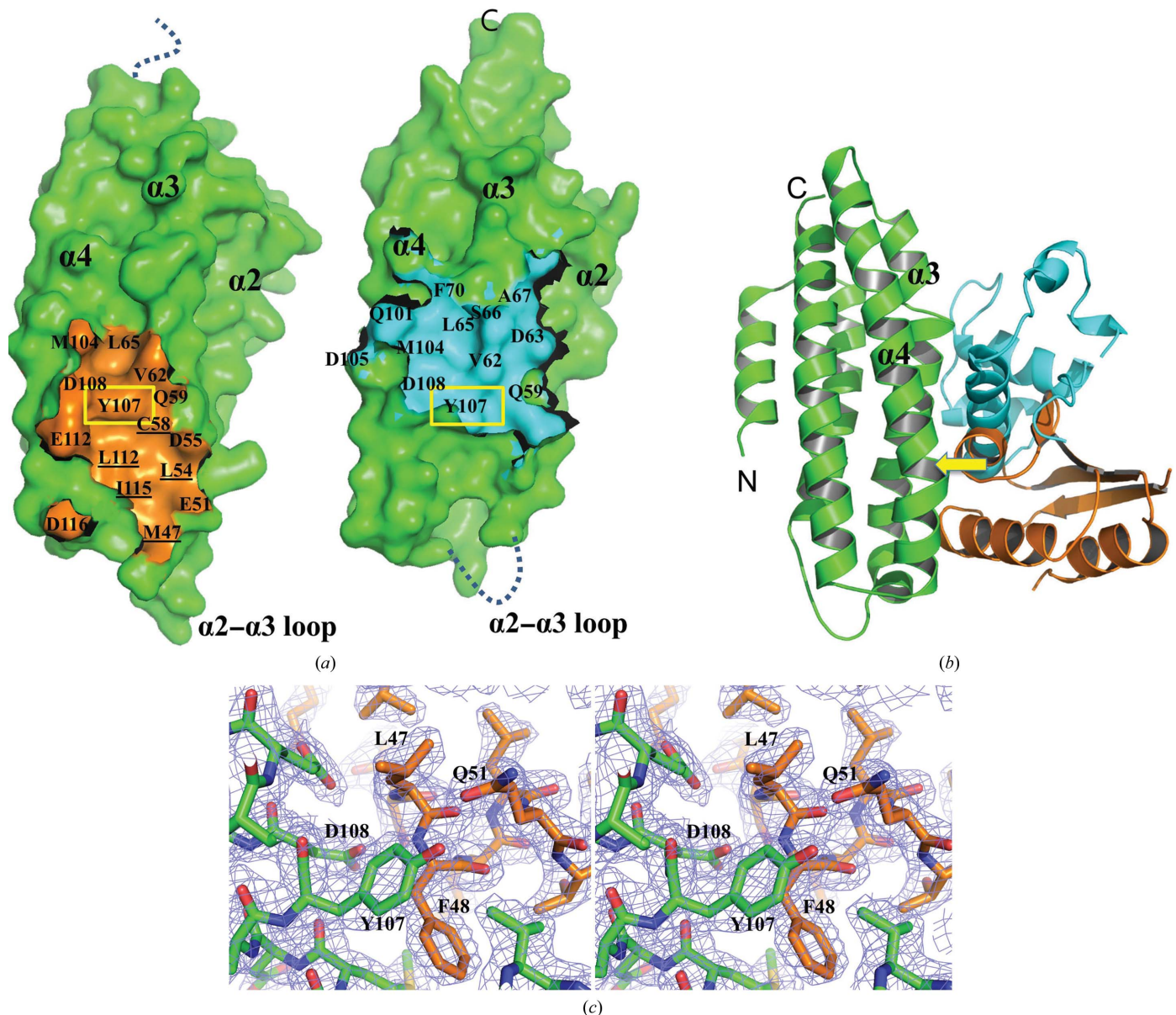


Figure 6 Binding of HPr to Rsd antagonizes the function of Rsd by competing with Rsd for σ^{70} . (*a*) Comparison of binding interfaces on Rsd with HPr (left) and σ^{70} (right). Surface representations of Rsd are shown in green. The binding interface with HPr is shown in orange (left) and that with σ^{70} is shown in cyan (right). Labels indicate the locations of major residues. The underlined residues are on the interface between Rsd and HPr and not on that between Rsd and σ^{70} , although they are not directly involved in interactions. Each Rsd molecule is aligned by the location of Tyr107, indicated by yellow squares. Disordered regions in the Rsd structures are displayed by broken lines. (*b*) Structural superposition of domain 4 of σ^{70} onto the Rsd–HPr structure. Domain 4 of σ^{70} is shown in cyan, Rsd is shown in green and HPr is shown in orange. The position of Tyr107 in Rsd is indicated by yellow arrows. (*c*) Stereo diagram of the electron-density map around Tyr107 of Rsd and Phe48 of HPr contoured at 1.0σ (blue mesh). Rsd is shown in green and HPr is shown in orange.

additional interactions with a few residues in the groove between $\alpha 2$ and $\alpha 3$ in the Rsd helical bundle (Westblade *et al.*, 2004).

Tyr107 and Asp108 of Rsd are involved in interactions with both HPr and σ^{70} . In the HPr–Rsd complex, Tyr107 and Asp108 of Rsd create a hydrogen-bonding network with HPr. Tyr107 of Rsd also makes hydrophobic interactions with the Leu47 and Phe48 residues of HPr (Fig. 3). A site-directed mutant of Rsd, Rsd(Y107A), was constructed to test whether Tyr107 of Rsd is crucial for interaction with HPr. Electrophoretic mobility shift assays using native PAGE, together with SPR experiments, revealed that the Y107A mutant did not form a complex with either HPr or σ^{70} (Figs. 5*a* and 5*b*, Table 4). In the complex structure of Rsd and domain 4 of σ^{70} , Tyr107 and Asp108 of Rsd form a hydrogen-bonding network with σ^{70} . The overlapping region in the binding interfaces of the Rsd–HPr and Rsd– σ^{70} complexes plays a critical role in the anti-Rsd function of HPr (Westblade *et al.*, 2004). Structural superposition indicates that HPr and σ^{70} bind to this overlapping region of Rsd in a mutually exclusive manner owing to steric hindrance (Fig. 6*b*). The intracellular concentration of dephosphorylated HPr can be up to eight times higher than that of σ^{70} depending on the availability of glucose (Park *et al.*, 2013). Therefore, we speculate that HPr can completely sequester Rsd from σ^{70} under conditions in which HPr predominantly exists in a dephosphorylated state, such as in cells growing exponentially in the presence of glucose.

4. Discussion

Rsd is a key regulator of global gene expression during the transition from exponential to stationary growth in bacterial cells (Jishage & Ishihama, 1998; Piper *et al.*, 2009). The binding between HPr and Rsd links nutrient availability and global gene expression (Park *et al.*, 2013). In this study, the binding interface between HPr and Rsd was visualized at atomic resolution. Subsequent biochemical and genetic experiments demonstrated that the structure reflects physiological interactions. The phosphorylation site at His15 of HPr is located on the edge of the binding surface of Rsd. This provides a molecular basis for the observation that only dephosphorylated HPr can interact with Rsd, thereby antagonizing the function of Rsd.

It should be noted that the σ^{70} -binding surface of Rsd only partially overlaps with the HPr-binding surface. Glu51, Met104 and Asp116 of Rsd are involved in specific binding to HPr. Met47, Leu54, Cys58, Leu112 and Ile115 of Rsd are also included in the HPr-binding interface (underlined residues in Fig. 6*a*, left), whereas Asp63, Ser66, Ala67, Phe70, Ser71, Gln101 and Asp105 of Rsd are only involved in the interaction with σ^{70} (Fig. 6*a*, right). When an amino-acid residue of Rsd involved in specific binding to HPr was mutated (Glu51 to Arg), the mutated Rsd still retained σ^{70} -binding activity, whereas HPr could not sequester the Rsd mutant protein from σ^{70} (Fig. 5). Therefore, the partial overlap of binding surfaces is sufficient for competition between HPr and σ^{70} for binding to Rsd.

HPr is a general PTS component that transfers a phosphoryl group from EI to the IIA subunit of sugar-specific EIIs. HPr also regulates glycogen phosphorylase through direct interaction in *E. coli* (Seok *et al.*, 1997). The solution structures of HPr in complexes with several partner proteins, EI (Garrett *et al.*, 1999), EIIA^{Glc} (Wang, Louis *et al.*, 2000), EIIA^{Mtl} (Cornilescu *et al.*, 2002), EIIA^{Man} (Williams *et al.*, 2005) and glycogen phosphorylase (Wang, Sondej *et al.*, 2000), have been solved. The interaction interfaces on HPr in different complexes overlap each other, and residues that are important for interaction with partner proteins are mainly located in helices $\alpha 1$ and $\alpha 2$. This study revealed that $\alpha 1$ and $\alpha 2$ of HPr form a binding interface with the lower part of $\alpha 3$ and $\alpha 4$ of Rsd (Fig. 1). The interactions are focused on a narrow surface and are mediated by both polar and hydrophobic interactions (Fig. 3). This finding suggests that a similar surface on HPr is involved in its interaction with other proteins, including Rsd.

Bacteria are exposed to various environments that are changing incessantly. Competition between sigma factors for core RNA polymerase is subject to tight genetic and biochemical regulation to prevent the untimely expression of genes directed by alternative sigma factors in the absence of stress or starvation. In this study, we have presented the detailed binding features of HPr and Rsd, explaining how the presence of glucose can facilitate gene expression governed by σ^{70} but prevent that governed by the stress-responsive sigma factor σ^S at the molecular level. Our findings explain the sophisticated bacterial gene-regulation mechanism integrating cellular and environmental information.

Acknowledgements

This research was supported by the R&D Convergence Center Support Program, Ministry for Food, Agriculture, Forestry and Fisheries, Republic of Korea (NCH), NRF 2010-0017384 funded by the Ministry of Science, ICT and Future Planning, Republic of Korea (YJS) and Grant NRF-2013R1A1A2007624 funded by the Ministry of Education, Republic of Korea (YHP). This study used beamline 5C at PLS (Pohang, Korea).

References

- Adams, P. D., Grosse-Kunstleve, R. W., Hung, L.-W., Ioerger, T. R., McCoy, A. J., Moriarty, N. W., Read, R. J., Sacchettini, J. C., Sauter, N. K. & Terwilliger, T. C. (2002). *Acta Cryst.* **D58**, 1948–1954.
- Barabote, R. D. & Saier, M. H. Jr (2005). *Microbiol. Mol. Biol. Rev.* **69**, 608–634.
- Blattner, F. R. *et al.* (1997). *Science*, **277**, 1453–1462.
- Braman, J., Papworth, C. & Greener, A. (1996). *Methods Mol. Biol.* **57**, 31–44.
- Chang, A. C. Y. & Cohen, S. N. (1978). *J. Bacteriol.* **134**, 1141–1156.
- Chen, V. B., Arendall, W. B., Headd, J. J., Keedy, D. A., Immormino, R. M., Kapral, G. J., Murray, L. W., Richardson, J. S. & Richardson, D. C. (2010). *Acta Cryst.* **D66**, 12–21.
- Cornilescu, G., Lee, B. R., Cornilescu, C. C., Wang, G., Peterkofsky, A. & Clore, G. M. (2002). *J. Biol. Chem.* **277**, 42289–42298.
- Debreczeni, J. É. & Emsley, P. (2012). *Acta Cryst.* **D68**, 425–430.
- DeLano, W. (2002). *PyMOL*. <http://www.pymol.org>.

- Deutscher, J., Aké, F. M. D., Derkaoui, M., Zébré, A. C., Cao, T. N., Bouraoui, H., Kentache, T., Mokhtari, A., Milohanic, E. & Joyet, P. (2014). *Microbiol. Mol. Biol. Rev.* **78**, 231–256.
- El-Kabbani, O. A. L., Waygood, E. B. & Delbaere, L. T. J. (1987). *J. Biol. Chem.* **262**, 12926–12929.
- Garrett, D. S., Seok, Y. J., Peterkofsky, A., Gronenborn, A. M. & Clore, G. M. (1999). *Nature Struct. Biol.* **6**, 166–173.
- Herzberg, O., Reddy, P., Sutrina, S., Saier, M. H. Jr, Reizer, J. & Kapadia, G. (1992). *Proc. Natl Acad. Sci. USA*, **89**, 2499–2503.
- Jia, Z., Quail, J. W., Delbaere, L. T. J. & Waygood, E. B. (1994). *Biochem. Cell Biol.* **72**, 202–217.
- Jia, Z., Quail, J. W., Waygood, E. B. & Delbaere, L. T. J. (1993). *J. Biol. Chem.* **268**, 22490–22501.
- Jishage, M. & Ishihama, A. (1998). *Proc. Natl Acad. Sci. USA*, **95**, 4953–4958.
- Jung, Y.-S., Cai, M. & Clore, G. M. (2012). *J. Biol. Chem.* **287**, 23819–23829.
- Koo, B.-M., Yoon, M.-J., Lee, C.-R., Nam, T.-W., Choe, Y.-J., Jaffe, H., Peterkofsky, A. & Seok, Y.-J. (2004). *J. Biol. Chem.* **279**, 31613–31621.
- LaVallie, E. R., DiBlasio, E. A., Kovacic, S., Grant, K. L., Schendel, P. F. & McCoy, J. M. (1993). *Nature Biotechnol.* **11**, 187–193.
- Lee, C.-R., Cho, S.-H., Kim, H.-J., Kim, M., Peterkofsky, A. & Seok, Y.-J. (2010). *Mol. Microbiol.* **78**, 1468–1483.
- Lee, C.-R., Cho, S.-H., Yoon, M.-J., Peterkofsky, A. & Seok, Y.-J. (2007). *Proc. Natl Acad. Sci. USA*, **104**, 4124–4129.
- Liao, D.-I., Silverton, E., Seok, Y.-J., Lee, B. R., Peterkofsky, A. & Davies, D. R. (1996). *Structure*, **4**, 861–872.
- Lux, R., Jahreis, K., Bettenbrock, K., Parkinson, J. S. & Lengeler, J. W. (1995). *Proc. Natl Acad. Sci. USA*, **92**, 11583–11587.
- Mitchell, J. E., Oshima, T., Piper, S. E., Webster, C. L., Westblade, L. F., Karimova, G., Ladant, D., Kolb, A., Hobman, J. L., Busby, S. J. & Lee, D. J. (2007). *J. Bacteriol.* **189**, 3489–3495.
- Nam, T.-W., Jung, H. I., An, Y. J., Park, Y.-H., Lee, S. H., Seok, Y.-J. & Cha, S.-S. (2008). *Proc. Natl Acad. Sci. USA*, **105**, 3751–3756.
- Napper, S., Delbaere, L. T. J. & Waygood, E. B. (1999). *J. Biol. Chem.* **274**, 21776–21782.
- Otwinowski, Z. & Minor, W. (1997). *Methods Enzymol.* **276**, 307–326.
- Park, Y.-H., Lee, C.-R., Choe, M. & Seok, Y.-J. (2013). *Proc. Natl Acad. Sci. USA*, **110**, 21142–21147.
- Park, Y.-H., Lee, B. R., Seok, Y.-J. & Peterkofsky, A. (2006). *J. Biol. Chem.* **281**, 6448–6454.
- Patikoglou, G. A., Westblade, L. F., Campbell, E. A., Lamour, V., Lane, W. J. & Darst, S. A. (2007). *J. Mol. Biol.* **372**, 649–659.
- Piper, S. E., Mitchell, J. E., Lee, D. J. & Busby, S. J. (2009). *Mol. Biosyst.* **5**, 1943–1947.
- Postma, P. W., Lengeler, J. W. & Jacobson, G. R. (1993). *Microbiol. Rev.* **57**, 543–594.
- Reddy, P., Peterkofsky, A. & McKenney, K. (1989). *Nucleic Acids Res.* **17**, 10473–10488.
- Seok, Y.-J., Lee, B. R., Zhu, P.-P. & Peterkofsky, A. (1996). *Proc. Natl Acad. Sci. USA*, **93**, 347–351.
- Seok, Y.-J., Sondej, M., Badawi, P., Lewis, M. S., Briggs, M. C., Jaffe, H. & Peterkofsky, A. (1997). *J. Biol. Chem.* **272**, 26511–26521.
- Sharma, U. K. & Chatterji, D. (2008). *J. Bacteriol.* **190**, 3434–3443.
- Vagin, A. & Teplyakov, A. (2010). *Acta Cryst. D* **66**, 22–25.
- Wang, G., Louis, J. M., Sondej, M., Seok, Y.-J., Peterkofsky, A. & Clore, G. M. (2000). *EMBO J.* **19**, 5635–5649.
- Wang, G., Sondej, M., Garrett, D. S., Peterkofsky, A. & Clore, G. M. (2000). *J. Biol. Chem.* **275**, 16401–16403.
- Weigel, N., Powers, D. A. & Roseman, S. (1982). *J. Biol. Chem.* **257**, 14499–14509.
- Westblade, L. F., Ilag, L. L., Powell, A. K., Kolb, A., Robinson, C. V. & Busby, S. J. (2004). *J. Mol. Biol.* **335**, 685–692.
- Williams, D. C. Jr, Cai, M., Suh, J.-Y., Peterkofsky, A. & Clore, G. M. (2005). *J. Biol. Chem.* **280**, 20775–20784.
- Winn, M. D. *et al.* (2011). *Acta Cryst. D* **67**, 235–242.